Deep HDS of diesel fuel: chemistry and catalysis

Teh C. Ho

Corporate Strategic Research Labs, ExxonMobil Research and Engineering Co., Annandale, NJ 08801, USA

Available online 11 September 2004

Abstract

The sulfur specification for diesel fuel has been tightened exponentially over the years. In the near future, the specification will go down below 10 ppmw or less. A fundamental question then is whether the goal of reaching such ultralow sulfur regime will scale exponentially in difficulty. To help answer this question, this paper aims to identify limiting factors bearing on the chemistry and catalysis in this regime. The emphasis is on low-pressure operation. Among the topics discussed are: reactivity–property relationships, catalyst functionalities, inhibiting effects, poisoning dynamics, nature of active sites, and bulk transition metal sulfides. It is shown that certain bulk metal sulfides are intrinsically active and selective for desulfurizing 4-substituted and 4,6-disubstituted dibenzothiophenes.
© 2004 Elsevier B.V. All rights reserved.

Keywords: Refractory sulfur compounds; HDS kinetics and catalysis; Transition metal sulfides; Process modeling; Deep HDS process

1. Introduction

This paper focuses on deep hydrodesulfurization (HDS) of petroleum middle distillates (200–370 °C boiling range) for manufacturing diesel fuel. The US Environmental Protection Agency Tier II regulations require that on-road diesel's sulfur specifications be lowered to 15 ppmw by June 2006, down from the current 500 ppmw. The present EU specification is expected to be below 50 ppmw in 2005 and about 10 ppmw around 2008. To put this trend in perspective, Fig. 1 shows a "first-order kinetic plot" (semi-log) for the diesel sulfur specifications (US, EU, and Japan). The plot is only illustrative and the scales are not exact. It shows that to a good approximation the sulfur specification has been tightened exponentially over the years.

The sulfur content of unhydrotreated middle distillates, or *raw distillates*, typically ranges between 1 and 3 wt.%, using round numbers. Desulfurizing such distillates to the 10–15 ppmw levels is a formidable challenge—especially at low hydrogen pressures. Due to the current 350–500 ppmw specifications mandated in several countries, today many desulfurized middle distillates have a low total sulfur content but a disproportionately high concentration of refractory sulfur species. To desulfurize these *prehydrotreated distil-*

lates requires different catalysts and operating conditions than those used for deep HDS of raw distillates. Great strides have been made in exploring various two-stage process options ([1] and references therein).

Most existing distillate HDS processes have been optimized for treating raw distillates to meet the 350–500 ppmw specifications. To stretch today's technology to the ultralow sulfur regime requires overcoming the difficulty of desulfurizing 4-substituted and 4,6-disubstituted diben-zothiophenes. These species are the most refractory sulfur heterocycles and collectively may be called β-DBTs for short, because the 4 and 6 positions are β to the sulfur atom. The refractoriness of β-DBTs arises from the steric hindrance around the sulfur atom [2,3].

Much of the information on the HDS of non-β-DBTs and β-DBTs can be found in several books and recent reviews [1,4–14]; five of the reviews appeared in 2003. This paper is a synopsis of some recently published and unpublished results obtained in our laboratory. A prevailing theme is low-pressure HDS of β-DBTs because of its technical challenge. Results are obtained from raw distillates, prehydrotreated distillates, and model compounds. Among the topics discussed are: reactivity–property relationships, catalyst functionalities, inhibiting effects (organonitrogen, H_2S, thermodynamics, hydrogen solubility), kinetics modeling, nature of active sites, and bulk metal sulfides. To set the
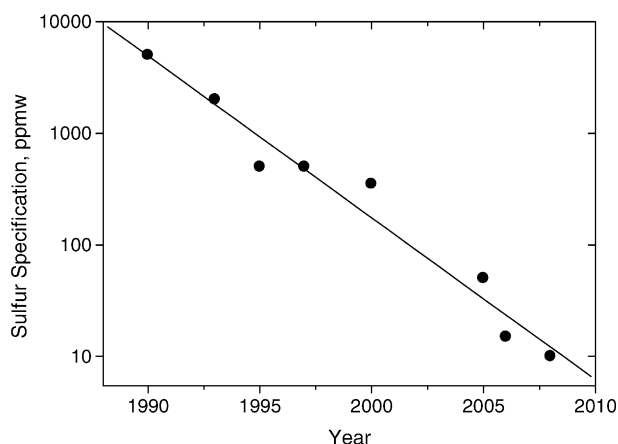
Fig. 1. On-road diesel sulfur specification (logarithmic scale) vs. calendar year.

stage, we begin with a broad-brush overview of some key aspects of deep HDS of diesel fuel, a term synonymous with the HDS of β-DBTs.

2. Overview

Industrial HDS has been largely carried out on sulfided CoMo/Al$_2$O$_3$ or NiMo/Al$_2$O$_3$. The most important catalytically active sites are believed to be sulfur anion vacancies associated with exposed Mo cations. The catalytic properties of these sites depend strongly on the neighboring promoter metals Co and Ni in the so-called Co(Ni)–Mo–S structures [7,8]. These coordinatively unsaturated sites occur at the edges and corners of MoS$_2$ crystallites. For simplicity, it is common to group such active sites into two broad categories in terms of functionality: one primarily for hydrogenation and the other primarily for hydrogenolysis. Another broad classification is based on the stacking height of MoS$_2$ [7,8]. Type I sites are found on monolayer MoS$_2$ slabs, while Type II sites on multilayered slabs. The MoS$_2$ portion of the active phase has a structure essentially identical to that of conventional MoS$_2$. It is believed that surface SH groups, located at the MoS$_2$ edges [7], provide much of the hydrogen needed for hydroremoval and hydrogenation reactions.

Alkyldibenzothiophenes can be desulfurized along two different paths. The hydrogenolysis path gives biphenyl-type products (BP) through direct sulfur extraction. The hydrogenation path produces cyclohexylbenzene-type products (CHB) through prehydrogenation of one of the aromatic rings. The relative importance of these two paths may be gauged by the ratio of their rate constants. But this ratio is not easily available. A rough hydrogenation index γ may be defined as the mass ratio of CHB to BP in the desulfurized product, namely

$$\gamma = \frac{\text{wt.\% CHB in product}}{\text{wt.\% BP in product}} \qquad (1)$$

This definition needs some clarification. For the HDS of 4,6-diethyldibenzothiophene (46DEDBT), γ is the ratio of C4CHB (diethylcyclohexylbenzenes and isomers) to C4BP (diethylbiphenyls and isomers), although C2CHB (ethylcyclohexylbenzene and dimethylcyclohexylbenzenes) and C2BP (ethylbiphenyl and dimethylbiphenyls) are minor products [15]. Similarly, in the HDS of 4,6-dimethyldibenzothiophene (46DMDBT), γ is the ratio of C2CHB to C2BP. Comparing γ for different catalysts is meaningful only at constant HDS. Fortunately, at least for highly hindered β-DBTs (e.g., 46DEDBT), γ does not vary much with space velocity at constant temperature and pressure [15]. Since hydrogenolysis generally has a higher activation energy than hydrogenation [16–18], γ decreases with temperature. And γ increases with pressure because hydrogenation is a stronger function of hydrogen pressure [19].

Until recently, most commercial catalysts were optimized for the HDS of non-β-DBTs. The atomic ratio $r = M/(M + Mo)$ (M = Co, Ni) typically is less than 0.4. The effect of Co (Ni) is to increase the HDS rate through a drastic enhancement of catalyst's hydrogenolysis functionality [10,14,19,20]. When performing HDS, these low-γ catalysts do not consume much hydrogen.

A very different situation arises when it comes to the HDS of β-DBTs, which relies heavily on the hydrogenation route. The system is characterized by high γ [21,22]. The variation in HDS reactivity within β-DBTs is significant [21]. With the little hydrogenation power they possess, conventional catalysts generally require high hydrogen pressures or long contact times to attain an acceptable HDS rate. However, many refiners are limited by hydrogen pressure. Running HDS at too high a temperature jeopardizes diesel quality. To minimize capital investment and preserve crude slate flexibility, there is an enormous incentive to achieve deep HDS at low hydrogen partial pressures—hence the emphasis of this paper.

The nature of the steric hindrance in β-DBTs has been and continue to be a subject of debate. One view is that it retards the adsorption of β-DBTs on the catalyst surface [2,3,23]. This implies that the rate-limiting step lies in adsorption, suggesting an end-on adsorption mode involving interactions between the sulfur atom and active sites. An alternate view is that the steric hindrance slows down the surface C–S bond scission [19,24–26]. Here, the rate-limiting step lies not in sulfur-centered adsorption, suggesting a side-on adsorption mode involving the π-electrons of the aromatic ring. The steric effect has also been proposed to reduce the rate of oxidative addition of the C–S bond to the catalytic site [9] or to retard the adsorption of dihydrogenated β-DBTs [19].

As implied by high γ, the HDS of β-DBTs is a hydrogen intensive process, putting a premium on catalyst hydrogenation functionality. Existing Co(Ni)Mo/Al$_2$O$_3$ catalysts are hydrogenolysis selective. Directionally, decreasing the Co (Ni) loading should enhance the selectivity toward hydrogenation. Indeed, molybdenum sulfide by itself,

supported or not, is more selective for hydrogenation compared to its Co (Ni) promoted analogs [10,19,20,26]. Bataille et al. [19] reported that 46DMDBT over Mo/Al$_2$O$_3$ is more easily hydrogenated and hence more reactive than DBT. Pyridine adsorption is much higher on unpromoted catalysts than on promoted catalysts, suggesting that the former is more acidic [20]. The disadvantage of unpromoted molybdenum sulfide catalysts is their low activity.

There is an extensive literature on various aspects of catalyst support in the context of deep HDS. The reader is referred to a special issue of *Catalysts Today* (vol. 86, 2003) for recent developments. Many researchers have explored ways of modifying γ-Al$_2$O$_3$ (e.g., SiO$_2$-Al$_2$O$_3$, P$_2$O$_5$-Al$_2$O$_3$, F-Al$_2$O$_3$, TiO$_2$-Al$_2$O$_3$, Pt-Al$_2$O$_3$) or developed non-traditional supports for HDS. Examples: SiO$_2$, ZrO$_2$-TiO$_2$, carbon, zeolites, and mesoporous materials (e.g., MCM-41). Incorporation of a solid acid into the support helps adsorption and also promotes hydrogenation through protonation followed by hydride transfer [27]. A solid acid may also isomerize β-DBTs into non-β-DBTs, thus speeding up sulfur removal on conventional catalysts. However, such acid-assisted catalysts are prone to coking and poisoning by organonitrogen. Developing new supported catalysts is complicated by the need to characterize metal–support interactions.

A simpler yet less researched avenue is to explore bulk transition metal sulfides. Model-compound studies have indicated that they are hydrogenation selective [28]. Many bulk Mo(W)S$_2$-based sulfides are quite active and selective toward hydrodenitrogenation (HDN), an attribute that goes hand in hand with hydrogenation functionality [29–31]. Highly hydrogenative catalysts in general are sensitive to hydrogen pressure. They require a commensurately fast supply of surface hydrogen, which is believed to come largely from heterolytic dissociation of hydrogen [7,32,33]. At low hydrogen pressures, it may well turn out that this dissociation reaction and/or the transport of hydrogen to the active sites become the limiting factor. The latter may be the result of low solubility and/or slow mass transfer of hydrogen in the fluid phase.

Prehydrotreated and raw distillates have very different compositions and properties. Obviously, a matter of great concern in commercial HDS is the inhibiting effects of nitrogen species, aromatics, and H$_2$S. For instance, the rate constant of 46DMDBT HDS decreases by a factor of 10 in going from a straight run distillate to a light catalytic cycle oil (LCO) [34]. This points to the importance of exploring quantitative property–reactivity relationships from real-feed experiments.

3. Property–reactivity relationships

Petroleum fractions are known for their daunting complexities. To gain insights into commercial HDS processes, one common approach has been to study the catalytic chemistry with selected probe molecules and then

pieces together the results to infer some aspects of real feed HDS. This approach in many cases fails to capture the dominant aspects of the process. An alternative approach, as taken here, is motivated by the observation that process and catalyst developers often have at their disposal pilot plant and commercial data on various feeds and catalysts. Mining of these databases may provide property–reactivity correlations that help design critical model-compound experiments.

Two property–reactivity correlations have been developed: one for raw distillates [35] and the other for prehydrotreated distillates [36]. Briefly, the data mining technique used consists of two steps. First, the raw data are projected onto a low-dimensional space by means of chemometrics [37]. The purposes are to: (1) gain insights into the underlying chemistry and identify dominating subprocesses, and (2) eliminate variable redundancy (cross correlation) and noise contributions. The next step is to construct simple correlations in terms of dominant yet readily accessible properties, as discussed below.

3.1. Raw distillates

A total of 13 specially selected high-sulfur (0.9–3.2 wt.%) raw distillates were desulfurized over a CoMo/Al$_2$O$_3$ catalyst at 343 °C and 1.83 MPa hydrogen pressure. Each feed was characterized by 24 physicochemical properties. Due to the wide reactivity spectrum, the product sulfur level ranges from 95 ppmw to 1.1 wt.%. Chemometric analysis reveals that the HDS reactivity, defined as the 1.5-order volumetric rate constant, is dominated by the following three properties in order of decreasing importance: degree of feed saturation ≫ DBTs self-inhibition > organonitrogen poisoning. This leads to the following property–reactivity correlation in terms of API gravity (API), and concentration of DBTs (DBT + β-DBTs), and feed nitrogen content (N_f) [35]:

$$\text{HDS reactivity} = (\text{API})^{2.18}(\text{DBTs})^{-0.31}(N_f)^{-0.2} \qquad (2)$$

Thus, the API gravity is by far the most important determinant of reactivity. Bearing in mind that here we deal with low-pressure HDS of widely different feeds with aromatic contents ranging from 22 to 69 wt.%. Also, the API gravity to some extent reflects feed heaviness [35] and is the most important determinant of hydrogen solubility in oils.

Schultz et al. [38] tested five raw distillates and one prehydrotreated distillate on a CoMo/Al$_2$O$_3$ catalyst and concluded that feed sulfur content is the best indicator of HDS reactivity. The six feeds are all of high quality because of their high and fairly constant API gravity (32.9–41 versus 16.5–38.6 in Ref. [35]) and low nitrogen content (60–509 ppmw versus 12–2061 ppmw in Ref. [35]). This, coupled with the high pressure (5 MPa) used in the experiments, explains Schultz et al.'s conclusion.

Using the temperature required to achieve 500 ppmw product sulfur (T_{500}) as the reactivity index, Shih et al. [39]

developed the correlation: $T_{500} = 454\,°F + 31\,°F\,\exp(S_{600F+})$ + $25\,°F\,\ln(N_f)$, S_{600F+} being the sulfur content (wt.%) of the $600\,°F$-plus fraction of the feed. Thus, the concentration of heavy sulfur is far more influential than the organonitrogen concentration. The correlation does not have a term reflecting the overall feed quality such as measured by the API gravity. This may be rationalized by two observations. One is that there is a certain degree of inverse correlation between S_{600F+} and API gravity. Another is that the experiments were done at a high hydrogen pressure (4.5 MPa) and hence a fast rate of aromatic hydrogenation. This is especially relevant given the low-nitrogen content (maximum 870 versus 2061 ppmw in Ref. [35]) of the feeds.

The above begs the question: upon dropping the API gravity term, can Eq. (2) correlate Shih et al.'s data? To answer this question, we scale the T_{500} reactivity data with an Arrhenius-type equation, since the reactivity in Eq. (2) is based on the rate constant (constant temperature). The rescaled reactivity (R_{HDS}) takes the form $R_{HDS} = a\,\exp(b/T_{500})$ (T_{500} in $°K$). With S_{600F+} as a proxy for DBTs, an alternative correlation based on the form of Eq. (2) is: $R_{HDS} = (S_{600F+})^{-0.31}(N_f)^{-0.2}$. Fig. 2 shows that this equation correlates the data with just two fitting parameters: $a = 8 \times 10^{-4}$ and $b = 5393.8$. Shih et al.'s correlation has three parameters.

3.2. Prehydrotreated feeds

A total of 13 specially selected prehydrotreated distillates were tested at 4.6 MPa over a sulfided NiMo/Al$_2$O$_3$ catalyst. Each feed was characterized by 10 properties. Feed nitrogen content (ppmw) was found to be far more influential than any other feed property. A linear function can satisfactorily correlate the data [36], that is,

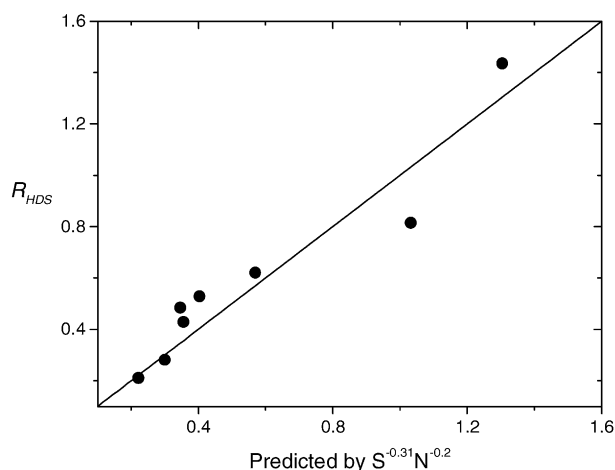$$\text{HDS reactivity} = u - vN_f \qquad (3)$$

Fig. 2. Predicted vs. measured HDS reactivity of raw distillates. $R_{HDS} = a\,\exp(b/T_{500}) = (S_{600F+})^{-0.31}(N_f)^{-0.2}$. Data are taken from [39].

Here, the reactivity is measured by 1.2-order volumetric HDS rate constant and the two fitting parameters u and v depend on catalyst and conditions. The linear dependence can be derived from a Langmuir competitive adsorption model [36].

The above result is explained as follows. First, the nitrogen species in question are ones that survive the first stage hydrotreatment. Most of them are partially or fully hydrogenated species that are more inhibiting than those in the parent raw feeds. For instance, in the case of six-membered nitrogen heterocycles, tetrahydroquinoline is a stronger inhibitor than quinoline in the HDS of 46DEDBT or DBT [40]. Five-membered nitrogen heterocycles such as alkylcarbazoles tend to survive the first stage hydrotreatment, since they cannot compete with six-membered nitrogen species for HDN sites [41]. If some five-membered nitrogen heterocycles do get hydrogenated in the first stage treatment, they become more poisonous [41]. Prehydrotreated distillates contain a disproportionately high concentration of alkylcarbazoles [12,42–44].

Second, prehydrotreated distillates are low in total sulfur. This, coupled with the low adsorptivity of β-DBTs (more on this later), greatly diminishes sulfur's self-inhibiting effect. Finally, prehydrotreated feeds have a relatively low level of polynuclear aromatics (PNA), most of which are likely two-ring aromatics. Naphthalene is a much weaker poison than alkylcarbazoles in the HDS of 46DEDBT [15].

Similar observations have been made by others. Van Looij et al. [45] blended two severely prehydrotreated distillates in different proportions and spiked the blended feeds with DBT to obtain model distillates containing 2000 ppmw total sulfur. With either CoMo/Al$_2$O$_3$ or NiMoP/Al$_2$O$_3$, these feeds showed a -0.15 power-law inhibitory effect of traces of basic nitrogen ($N_f < 30$ ppmw). In separate experiments, the prehydrotreated distillates were spiked with naphthalene (0.95 wt.% in total feed), chrysene (0.013 wt.%), tetralin (0.07 wt.%), and pyrene (0.53 wt.%). These added PNA show little if any inhibitory effect. Mochida and coworkers [42] found that organonitrogen is a more potent poison in β-DBTs HDS than in DBT HDS and that organonitrogen in prehydrotreated feed has a very strong effect on subsequent HDS [12,42].

On the basis of the foregoing, the correlations developed by Schultz et al. [38] and Shih et al. [39] may be viewed as special cases of Eq. (2). Furthermore, Eq. (2), when applied to the HDS of prehydrotreated distillates, does point to the dominance of feed nitrogen content [36]. In view of all this, the qualitative features embodied in Eq. (2), derived from widely different feeds under rather unfavorable conditions (low hydrogen pressure), do appear to have some generality.

3.3. Alkylcarbazoles

The picture that emerges is that while nitrogen species have long been known to inhibit the HDS of non-β-DBTs, their effect becomes more pronounced in the HDS of β-

DBTs. One implication for catalyst development seems that the higher the activity for the HDS of β-DBTs is, the stronger the response to nitrogen poisoning [42]. As noted earlier, alkylcarbazoles plays a dominant role in the HDS of prehydrotreated distillates. And they are also the predominate nitrogen species in refractory raw distillates (e.g. LCO) [46–49]. Shin et al. [50] did not find acridine in LCO and reported the following HDN reactivity order: indole > methylanilines > methylindoles > quinoline > carbazole > methylcarbazoles. There is evidence to suggest that the rate-limiting step in the HDN of alkylcarbazoles may lie in the hydrogenation of alkylcarbazoles [41,51].

Alkylcarbazoles are harder to denitrogenate than carbazole [42]. Among alkylcarbazoles in real feeds, 1-methylcarbazole has the highest concentration [43]. The HDN reactivity of alkylcarbazoles decreases with the number of methyl substituent. Of mono-methylcarbazoles, 1-methylcarbazole has the lowest HDN reactivity [50]. Relative to the HDS of alkyl-DBTs, steric hindrance plays a less important role in determining the HDN reactivity of alkylcarbazoles [42,43]. The same is true of the HDN of methylindoles [52]. Alkylcarbazoles and their derivatives, whether electron rich or deficient, are very potent inhibitors for the HDS of 46DEDBT [15].

The above observations clearly make a strong case for taking a detailed look at the inhibiting effect of alkylcarbazoles on the HDS of β-DBTs. Before addressing this subject, a word about the effect of H_2S is in order.

3.4. Effect of H_2S

Hydrogenolysis is known to be more vulnerable to H_2S poisoning than hydrogenation [5,7,10,16,19]. Given the importance of hydrogenation to the HDS of β-DBTs, a hitherto under-appreciated point is that H_2S may in some cases actually enhance hydrogenation. This was observed with DBT HDS on bulk MoS_2 [53] and on $CoMo/Al_2O_3$ [54]. A similar observation was made in the HDS of 46DMDBT over NiMo/C [16,17]. This could be the result of an increased surface SH groups due to H_2S dissociation [7]. For perspective, H_2S inhibits aromatic hydrogenation [7]. In the HDN of six-membered nitrogen heterocycles, H_2S moderately inhibits hydrogenation but can enhance the C–N bond scission [41].

The point of note is that the inhibiting effect of H_2S is less pronounced in the HDS of β-DBTs than in the HDS of DBT [17,19,55]. This is consistent with the fact that hydrogenation plays a more important role than hydrogenolysis in the HDS of β-DBTs. Even in the HDS of raw distillates, the effect of H_2S is of secondary importance [35].

4. Deep HDS at low pressures

Given that the HDS of β-DBTs is hydrogen intensive, deep HDS of middle distillates at low hydrogen pressures

may be severely limited by at least three factors. The first has to do with the supply of hydrogen to the catalyst surface where hydrogen is activated and dissociated. The catalyst surface may be starved of adsorbed hydrogen due to low hydrogen solubility and/or slow mass transfer (especially in small laboratory reactors). Under most diesel HDS conditions, the reaction takes place in the liquid phase caused by capillary condensation. Second, the β-DBTs HDS rate may be limited by thermodynamic equilibrium at high temperatures. Third, the HDN rate, being sensitive to H_2 pressure, may be so slow that nitrogen compounds block virtually all active sites that are otherwise available for HDS.

4.1. Hydrogen supply

Hydrogen solubility in hydrocarbon solvents increases with increasing temperature. Hydrogen also has a relatively high kinematic viscosity. Fig. 3 shows the solubility as a function of solvent structure. It decreases in the following order: hexadecane > bicyclohexyl > tetralin > 1-methylnaphthalene [56–60]. Muroi et al. [61] observed that in the absence of a hydrocarbon solvent, the rates of DBT HDS and 46DMDBT HDS are lower than those in the presence of a solvent. Cyclohexane as a solvent yields a stronger rate enhancement than decaline. Importantly, the solvent effect is more pronounced for the HDS of 46DMDBT than that of DBT. The solvent effect observed by Muroi et al. corroborates the hydrogen solubility argument in that the solubility is a strong decreasing function of solvent's specific gravity. Muroi et al. explained their data in terms of diffusivity. The solvent effect was also observed in toluene hydrogenation [62].

In deep HDS catalyst screening studies, the disparity in catalyst activity among experimental catalysts generally diminishes with decreasing hydrogen pressure. This compression effect could be linked to hydrogen "starvation" as
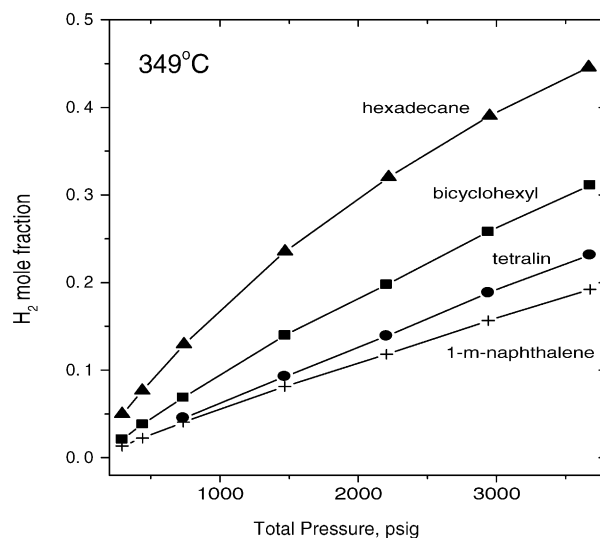

Fig. 3. Hydrogen solubility vs. hydrogen pressure for various hydrocarbon solvents at 349 °C [56–59].

the more hydrogenative catalysts would suffer more as the hydrogen pressure is decreased.

At a hydrogen pressure as low as 0.79 MPa, bulk RuS_2 at 343 °C desulfurizes an LCO from 1.47 wt.% to 220 ppmw versus 1680 ppmw obtained with a commercial HDS catalyst [63]. The remarkable performance of RuS_2 could be in part attributable to its isotropic cubic structure. The disulfide species $(S–S)^{-2}$ may increase the surface density of the SH groups resulting from facile heterolytic dissociation of hydrogen. And steric hindrance may become less of an issue for RuS_2 compared to catalysts based on MoS_2, which has a highly anisotropic layered structure.

Remarkable as the above result may be, the key remaining question is: Does hydrogen supply become an issue at low pressures when pushing to the 10–15 ppmw sulfur regime? Attempts have been made to eliminate potential hydrogen supply problem by using supercritical solvents [64]. This approach can be justified only if hydrogen supply is rate limiting at high pressures.

In the ensuing sections, we use the HDS of 46DEDBT over a sulfided CoMo/Al_2O_3-SiO_2 (catalyst A) to probe some fundamental aspects of deep HDS.

4.2. Potential thermodynamic limitation

The feed mixture used in the experiment contains 0.8 wt.% 46DEDBT in dodecane. The main HDS products are C4CHB, C4BP, C2CHB, C2BP, ethylbenzenes (C2BZ), and ethylcyclohexanes (C2CH) at 265 °C, 1.83 MPa, and 116 cc H_2/cc liquid feed. The overall HDS kinetics is pseudo-first order, suggesting a low site coverage. Also, $\gamma \sim$ 5.5 over a wide range of HDS levels, indicative of insignificant interconversion between C4BP and C4CHB [15]. Farag et al. [65] also observed pseudo-first-order behavior for 46DMDBT HDS on a CoMo/C catalyst at 2.9 MPa. They found that the extent of 3,3′-dimethylbiphenyl hydrogenation is low.

Fig. 4 depicts a lumped HDS network [15]. The reversible character of the β-DBTs hydrogenation step may limit HDS due to the thermodynamically mandated low concentration of hydro-β-DBTs at low hydrogen pressures and high temperatures [14,65,66]. This limitation, if significant, may
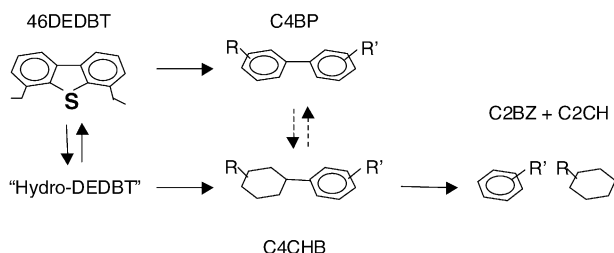
be particularly problematic at temperatures close to the end-of-the-run temperature and in the downstream zone of a commercial hydrotreater where hydrogen partial pressure is low. Farag et al.'s [65] MOPAC calculations indicated that at 2.9 MPa hydrogen pressure, the hydrogenation of 46DMDBT is favored at temperatures lower than 260 °C and becomes completely unfavored above 380 °C.

Experimentally, the extent of sulfur removal from 46DEDBT at a hydrogen pressure as low as 0.79 MPa is not equilibrium limited at least up to 400 °C. As Fig. 5 shows, the HDS level increases with temperature and essentially attains 100% at temperatures above 280 °C. Referring to Fig. 4, at high temperatures the "drainage" reaction "hydro-β-DBTs to hydrocarbons" become sufficiently fast, thus pulling the HDS reaction to the right. Also, some hydrogenation sites may convert to hydrogenolysis sites at high temperatures [15,16]. As noted before, γ decreases with temperature.

4.3. Poisoning by alkylcarbazoles

Due to its sufficiently high solubility, 3-ethylcarbazole (3ECBZ) was used as a model poison. Its inhibiting effect on 46DEDBT HDS was studied with two feed mixtures [15]. Feed A contains 0.8 wt.% 46DEDBT, while feed B contains 0.8 wt.% 46DEDBT and 0.112 wt.% 3ECBZ (80 ppmw as nitrogen atom). The experiments began with feed A at 265 °C and 1.83 MPa over catalyst A. After the catalyst lined out its activity (steady state I), feed A was replaced by feed B to start the poisoning experiment. Once the catalyst equilibrated its activity again (steady state II), feed A was put back on stream to strip the adsorbed poison off the catalyst. For comparison, the same set of experiments was done using 10 wt.% naphthalene as the poison.

Fig. 6 shows the HDS level versus h-on-stream, which is at a high 70% with feed A at steady state I but drops to about 10% at steady state II. By contrast, the damage caused by naphthalene is rather mild: HDS drops from 70% to 53%, even though the naphthalene concentration is orders of magnitude higher than that of 3ECBZ.
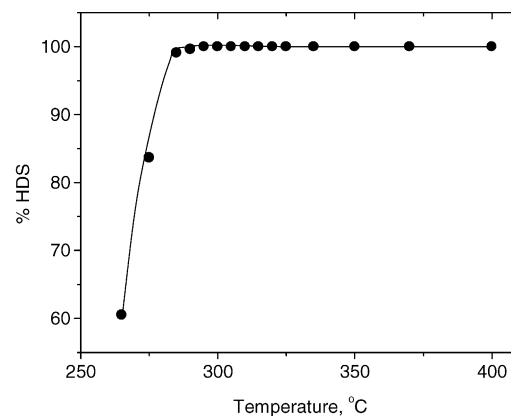

Fig. 4. Portion of lumped 46DEDBT HDS network at 265 °C and 1.83 MPa H_2 pressure. "Hydro-DEDBT" is the lump of all partially hydrogenated 46DEDBT. The R and R′ groups may or may not have the same carbon number [15].

Fig. 5. Percentage of HDS of 46DEDBT vs. temperature at 0.79 MPa hydrogen pressures; 1.5 WHSV, 116 cc H_2/cc liquid feed.
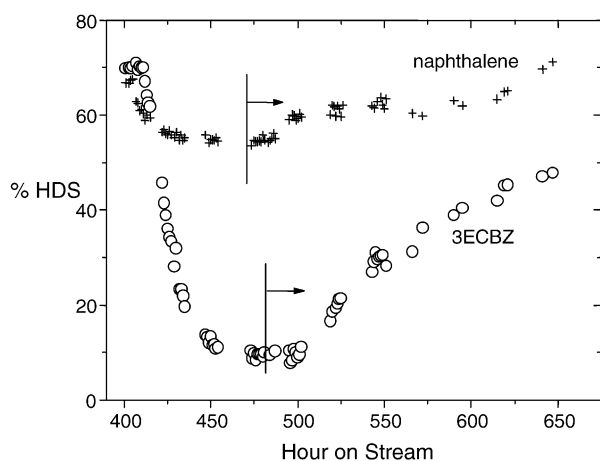
Fig. 6. Percentage of HDS vs. elapsed hr after introduction of 3ECBZ-containing feed (feed B) at the 400th hour; 1.83 MPa, 265 °C, 2.4 WHSV, 116 cc H_2/cc liquid feed; the vertical lines indicate the beginning of the stripping experiments using feed A [15].
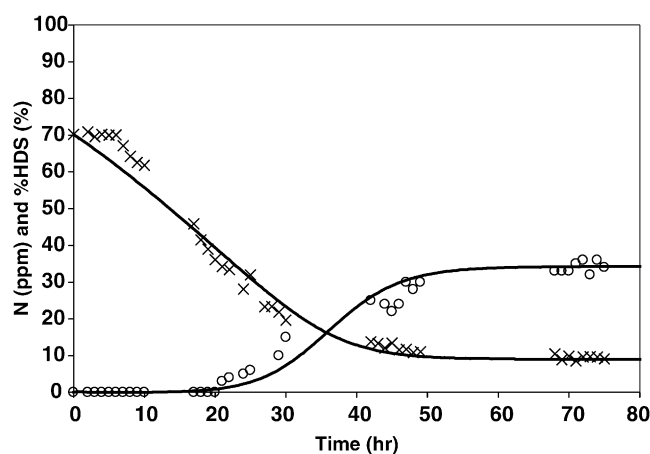

Fig. 7. Percentage of HDS and total nitrogen concentration at reactor exit as functions of elapsed time following introduction of 3-ethylcarbazole; 265 °C, 2.4 WHSV, 1.83 MPa, and 116 cc H_2/cc liquid feed. Solid curves are predicted from the non-equilibrium model [71].

The difference between the two inhibitors can further be seen from subsequent stripping experiments with feed A (indicated by the vertical lines in Fig. 6). The recovery of the HDS level in the naphthalene case appears to be a two-step process. The loosely adsorbed species are stripped off the catalyst surface followed by the removal of strongly adsorbed species. The lost HDS activity can almost be fully recovered. The HDS activity recovery in the 3ECBZ case appears to be a one-step process with a progressively slower recovery rate. A complete recovery of the lost HDS activity does not seem feasible even after a long time. Nitrogen heterocycles are known to have the tendency to polymerize and form coke [41,67,68].

It is not hard to see why 3ECBZ is a more potent inhibitor than naphthalene. First, the proton affinity, boiling point, and molecular size of 3ECBZ are all higher than those of naphthalene [69]. Second, 3ECBZ and 46DEDBT have a similar shape. On this point, we note that fluorene is more inhibiting than anthracene and phenanthrene in 46DMDBT HDS, possibly due to its molecular shape [70]. Both 3ECBZ and 46DEDBT should be adsorbed flat and likely require similar multivacancy clusters. The flat adsorption is in line with the notion that the heteroatom in 3ECBZ or 46DEDBT is not readily available for interacting with active sites (the extra pair of electrons in 3ECBZ's nitrogen atom is tied up in the π cloud of the ring). Third, the hydrogenation of 3ECBZ would produce more basic nitrogen species that are more inhibiting than 3ECBZ [41].

5. Poisoning dynamics

The above data have been used to construct a mathematical model to gain a quantitative understanding of the poisoning dynamics. Fig. 7 shows the breakthrough behavior of the system after a sudden step change in the feed nitrogen content from 0 to 80 ppmw. The breakthrough of nitrogen does not occur until around the 20th hour, after which the product nitrogen content takes an upward leap, giving rise to a 58% HDN at steady state II. The solid curves are model predictions to be discussed later.

The nomenclature for the model is as follows. For sulfur species, k_s, k'_s, and k_{HDS} are the adsorption constant, desorption constant, and surface HDS rate constant, respectively. The corresponding rate constants for nitrogen species are k_n, k'_n, and k_{HDN}. The sulfur and nitrogen (atom) concentrations in the fluid phase are S and N, with S_f and N_f being the feed concentrations, respectively. Also, q_n and q_s are the respective adsorbed concentrations. The total capacity for adsorption on active sites is q_m, so $\theta_n = q_n/q_m$ is the fractional coverage of adsorbed nitrogen. Ref. [71] describes a hierarchical modeling approach for developing the simplest possible theory to quantify what goes on in the fluid phase and on the catalyst surface. Some of the key results are discussed below.

5.1. Langmuir–Hinshelwood equilibrium model

To simplify matters, the classical quasi-equilibrium and quasi-steady state assumptions immediately come to mind. They require that the adsorption and desorption be in rapid equilibrium [$k_{HDS} \ll (k_s S_f, k'_s)$ and $k_{HDN} \ll (k_n N_f, k'_n)$] and that their time scales be much shorter than the reactor residence time. The latter means that the catalyst surface quickly relaxes to a steady state as the 3ECBZ-containing feed travels down the bed immediately after the poisoning experiment commences. Consequently, the local concentrations of adsorbed species are "instantaneously" driven by the fluid phase composition, that is, $q_s = K_S q_m S/(1 + K_N N + K_S S)$ and $q_n = K_N q_m N/(1 + K_N N + K_S S)$, where $K_N = k_n / k'_n$ and $K_S = k_s / k'_s$ are the adsorption equilibrium constants. Due to the dominance of nitrogen inhibition,

the sulfur inhibition term in the denominator can be dropped with impunity.

At steady state II, the model yields the familiar equilibrium-based Langmuir–Hinshelwood model

$$\text{WHSV}\frac{dS}{d\tau} = -\frac{k_{HDS}K_S q_m S}{1 + K_N N} \tag{4}$$

$$\text{WHSV}\frac{dN}{d\tau} = -\frac{k_{HDN}K_N q_m N}{1 + K_N N} \tag{5}$$

where $\tau = z/L$, with z and L being the axial distance from the reactor inlet and the reactor length, respectively.

Here, the nitrogen adsorption is so fast and strong that S, N, and θ_n behave as sharp waves moving at the fluid velocity. The predicted breakthrough time is nothing but the fluid residence time, about 10 min. This is far shorter than the 20 h breakthrough time observed experimentally. Thus the model simply cannot describe the sluggish breakthrough behavior depicted in Fig. 7—yet it surely can be made to match the steady state data [71]. Relaxing the quasi-steady-state assumption while retaining the quasi-equilibrium assumption indeed slows down the advancing poisoning wave, but fails to describe the nitrogen behavior. The reason is that, in reality, the adsorbed nitrogen is so "sticky" that it just cannot fulfil the fast equilibrium requirement. The same behavior was observed with pyridine as a poison in the HDS of benzothiophene [72] and thiophene [73]. The non-equilibrium model discussed below rectifies the problem.

5.2. Langmuir non-equilibrium model

The non-equilibrium model summarized here is possibly the simplest one that describes both the steady state and transient experiments. Analysis of the step-response data led to two key assumptions [71]. One is that sulfur species sparsely adsorb on the active sites. Another is that the desorption rates of sulfur and nitrogen species are much slower than the surface HDS and HDN rates. At steady state II, the model becomes

$$\text{WHSV}\frac{dS}{d\tau} = -\frac{k_s q_m S}{1 + \tilde{K}_n N} \tag{6}$$

$$\text{WHSV}\frac{dN}{d\tau} = -\frac{k_n q_m N}{1 + \tilde{K}_n N} \tag{7}$$

where $\tilde{K}_n = k_n/k_{HDN}$. Thus, the mathematical structure of Eqs. (4) and (5) is identical to that of Eqs. (6) and (7) in that they all are of the form $(\text{WHSV})dY_i/d\tau = -k_i Y_i/(1 + K_2 Y_2)$, with $i = 1$ and 2 (2 refers to nitrogen). With three fitting parameters k_i and K_2, either model would fit the steady state data well. Yet the two models have entirely different physical meanings. For instance, the inhibition coefficient K_N is a thermodynamic quantity, whereas $\tilde{K}_n$ is a kinetic one. They have different temperature dependencies. Most importantly, the assumptions underlying Eqs. (6) and (7) are valid for

both transient and steady state situations. Such is not the case with Eqs. (4) and (5).

The foregoing discussions give a telling example of a pitfall in kinetics modeling. That is, rate constants determined solely from steady state experiments may not be valid because they cannot describe the transient behavior of the system. It is relevant to point out that the heats of chemisorption of 4MDBT (19–20 kcal/mol) and 46DMDBT (21 kcal/mol) were reported to be higher than that of DBT (10 kcal/mol) over CoMo/Al$_2$O$_3$ and NiMo/Al$_2$O$_3$ catalysts [74]. These results were taken as indicating that β-DBTs adsorption is not hindered and surface reaction is rate limiting [10,74–76]. The caveat is that the heats of chemisorption were solely calculated from steady-state experiments using an equilibrium Langmuir-Hinshelwood model. As such, the surface reaction was assumed to be negligibly slow a priori with no justification.

5.3. Governing parameters

Fig. 7 shows that the agreement between the non-equilibrium theory (solid curves) and experiment is good. The corresponding parameters are: $k_s = 0.21$ cc/g S/s, $k_n = 1.91$ cc/g N/s, $k_{HDN} = 6.32 \times 10^{-6}$ s^{-1}, and $q_m = 0.0038$ g S or g N/g$_{cat}$. In addition, we note that $k_{HDS} \gg k_{HDN} \gg k_n'$ and $k_{HDS} \gg k_s'$.

The model identifies two dimensionless groups that govern the poisoning process at steady state II. They both are related to catalyst properties and can be determined from steady state experiments [71].

$$p \equiv \frac{k_s}{k_n} = \frac{\ln(S_{p2}/S_f)}{\ln(N_{p2}/N_f)} \tag{8}$$

$$g \equiv \frac{k_n N_f}{k_{HDN}} = \frac{N_f \ln(N_{p2}/N_f)}{(N_f - N_{p2})}\left(1 - \frac{\ln(S_{p1}/S_f)}{\ln(S_{p2}/S_f)}\right) \tag{9}$$

where S_{p2} and N_{p2} are the sulfur and nitrogen concentrations in the effluent liquid at steady state II and S_{p1} is the effluent sulfur concentration at steady state I.

Hence, p is the adsorptivity ratio reflecting the intrinsic adsorption affinity of 46DEDBT relative to that of 3ECBZ. Eq. (8) says that the extents of HDS and HDN are related to each other through a pth-power law, with p depending on temperature for a given catalyst. The parameter g is an index of poisoning intensity, because it is the ratio of nitrogen adsorption rate to surface HDN rate. Alkylcarbazoles severely limit deep HDS due to their sheer concentration (N_f), high adsorptivity (k_n), and low reactivity (k_{HDN}).

5.4. Spatiotemporal behavior

Fig. 8 shows the fractional sulfur concentration (S/S_f) in the fluid phase as a function of bed position at successive elapsed times. Initially ($t = 0$ h), the reactor sulfur profile in the absence of 3ECBZ shows an exponential decline.
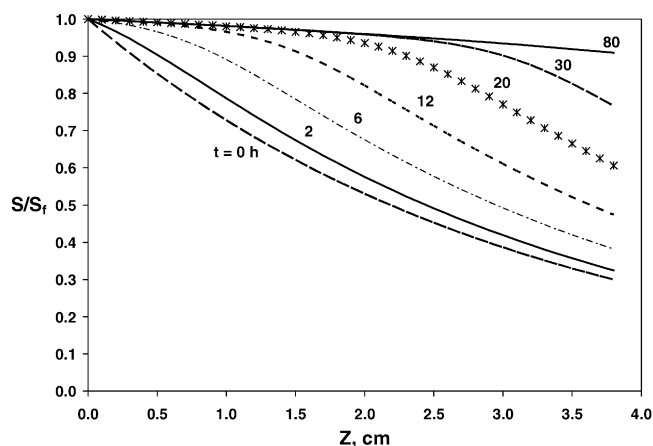
Fig. 8. Predicted moving sulfur concentration front S/S_f for different elapsed times [71].

Subsequently, the fluid sulfur content increases as the concentration wave travels toward the reactor outlet. The advancing sulfur front is not in local adsorption–desorption equilibrium with the active sites. The wave labeled with asterisks is for $t = 20$ h, approximately corresponding to the breakthrough time. After 30 h of nitrogen attack, the majority of the active sites in the bed are poisoned; the bulk of 46DEDBT stays in the fluid phase as a "bystander." As a result, the sulfur profile remains nearly flat and becomes only slightly concave downward near the reactor outlet where some active sites have not yet been poisoned at that moment. The sulfur concentration in reactor effluent increases as the poisoning proceeds.

Fig. 9 shows the fractional coverage of adsorbed nitrogen θ_n as a function of bed length at different elapsed times. The adsorption-reaction wave moves slowly toward the reactor exit. Initially, the catalyst in the upstream section of the bed partially depletes its active sites due to nitrogen uptake. In the downstream section, the catalyst surface is virtually free of adsorbed nitrogen species while sparsely occupied by sulfur species. At intermediate times, the catalyst near the
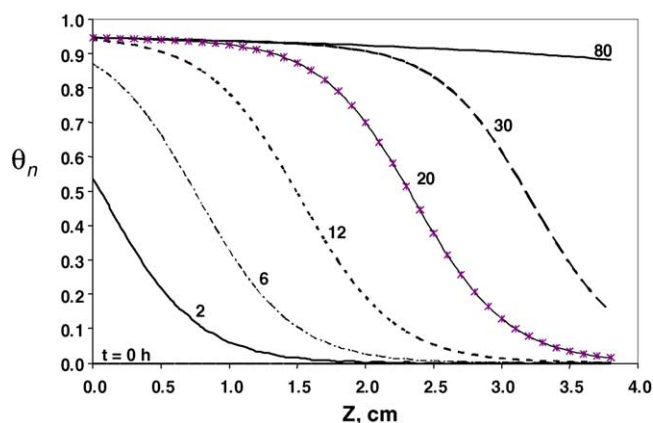

Fig. 9. Predicted fractional site coverage by adsorbed nitrogen, θ_n, for different elapsed times [71].

reactor inlet depletes almost all its active sites for 46DEDBT HDS, whereas that near the outlet partially depletes its active sites for HDS. Eventually, almost all of the sites are blocked off by nitrogen species. It is important to note that the model must account for surface HDN reaction; otherwise, it would not predict the nitrogen breakthrough curve *and* the steady state nitrogen concentration.

5.5. Some practical considerations

Eq. (9) says that $g = k_n N_f / k_{HDN}$ is a measurable poisoning intensity index. Correlating g with catalyst properties (e.g., metal composition, support type) should help catalyst development. As shown elsewhere [71], the nitrogen uptake θ_n is governed by the equation $\theta_n = g(N/N_f)/[1 + g(N/N_f)]$ at steady state II. Thus, θ_n is of order unity when $g \gg 1$ and of order g when $g \ll 1$. For typical middle distillates over commercial catalysts, $g > 10$. Thus, the real challenge is how to make $g \ll 1$. Several possible approaches are discussed below in light of Eqs. (6)–(9).

The controlling parameters for mitigating nitrogen's poisoning effect are k_n, k_s, k_{HDN}, N_f, and q_m. Decreasing k_n through modification of catalyst surface must be done in such a way that it would not hurt k_s, since the same sites are involved. Initial attempts to decrease k_n by modifying electronic and steric characteristics of carbazoles have not be successful [15]. Adjusting reaction temperature can lower g because k_n and k_{HDN} should in general have different temperature responses [15]. Lowering N_f through removing nitrogen species from distillates has been actively pursued [77–80]. Since k_{HDN} scales linearly with N_f for a constant g, a 10-fold increase in k_{HDN} (at constant k_n) means a 10-fold increase in the tolerance for the feed nitrogen level. Increasing q_m benefits both HDS and HDN. For low-pressure operation, a significant increase in q_m would require a commensurately fast supply of surface hydrogen.

6. Possible nature of active sites

As alluded to before, there has been no agreement on whether the steric hindrance around the sulfur atom retards 46DEDBT adsorption or C–S bond scission. The picture emerging here is that even in the absence of 3ECBZ, the adsorption of 46DEDBT is far slower than the surface HDS rate. The surface HDS reaction is so fast that 46DEDBT desorption becomes kinetically irrelevant over the time scale of interest.

If 46DEDBT is adsorbed vertically, it is not hard to see why adsorption is rate-limiting. It is not obvious why this should be the case with flat adsorption. One possible rationalization [15] is to posit that the structure of 46DEDBT is such that only a subset of active sites can fulfill the requirement for accommodating 46DEDBT adsorption and hydrogenation. The number of such sites, dubbed β sites, on catalyst A is so few that 46DEDBT has to "fish" for them.

Presumably, the β sites involve multiplets (or ensembles) of specifically arranged adjacent sulfur vacancies. Once a 46DEDBT molecule is adsorbed and hydrogenated, steric hindrance becomes significantly weakened and hence a facile C–S bond scission afterwards. As a consequence, the coverage of 46DEDBT on β sites is very low.

That 46DEDBT HDS is extremely sensitive to 3ECBZ [15] suggests that it does not take much 3ECBZ to break up the multiplets. In contrast, 3ECBZ is far less damaging in the HDS of DBT. DBT most likely adsorbs and reacts mainly on non-β sites. These observations suggest that 3ECBZ should favor β sites for its adsorption. Being an inhibitor for the HDS of β-DBTs [19], DBT can also adsorb and may even react on β sites.

A close look at Fig. 7 reveals that the non-equilibrium model underpredicts the HDS level for the initial part (0–5 h) of the prebreakthrough period. Within this short "induction" period the extent of HDS remains fairly constant. The existence of this induction period seems indicative of a low occupancy of the β sites. Initially, it is rare for 3ECBZ to "hit" an adsorbed sulfur species because there are so many bare β sites, thus severely limiting 3ECBZ's poisoning power. It is also possible that non-β sites could adsorb 3ECBZ. But this should be a secondary effect because 3ECBZ is relatively benign in DBT HDS. Neither situation is accommodated in the non-equilibrium model.

Notwithstanding their similarities (shape, adsorption mode/site, hydrogenation-dominated heteroatom removal), 46DEDBT and 3ECBZ have vastly different adsorptivities and reactivities (Section 5). A small fraction of the β sites give a high 70% HDS at steady state I, versus a 58% HDN over a lot of β sites at steady state II (Fig. 9). Thus the surface turnover rate for the HDS of 46DEDBT must be far greater than that for the HDN of 3ECBZ. On the other hand, 46DEDBT has a much weaker affinity for β sites than 3ECBZ ($p = 0.11$). The catalyst can adsorb 3ECBZ at a rate at least 17-fold faster than it can denitrogenate 3ECBZ ($g = 17.4$).

The above arguments, albeit heuristic, suggest that 46DEDBT may not be inherently more refractory than DBT—if a catalyst has a sufficiently high surface density of β sites. This leads to the topic of the next section, which shows that certain bulk metal sulfides are far more active than commercial catalysts for desulfurizing β-DBTs.

7. Bulk metal sulfides

As noted earlier, bulk transition metal sulfides (TMS) tend to be more hydrogenation selective than supported catalysts. A strategy for preparing TMS is to incorporate promoter metals into the Mo(W)S$_2$ edge planes through synthesis of molecular complexes or direct reaction [81]. The structure of the molecular complexes contains fragments that may possibly resemble those in TMS [81]. Several families of catalysts have been developed using this

approach. One example is the catalysts prepared from the thermal decomposition of the so-called "butterfly compounds" which are various salts of $Co(MoS_4)_2^{2-}$ and $Ni(MoS_4)_2^{2-}$ [82,83]. In these compounds, the promoter metal(s) and Mo are covalently bound. Another example is the chemical "decoration" of MoS$_2$ edge via a facile reaction between MoS$_2$ with Co$_2$(CO)$_8$ leading to a rapid evolution of CO at room temperature [84–86]. A third example is the catalysts derived from the thermal decomposition of metal amine thiomolybdates in which the promoter metals and Mo are molecularly associated with each other [29–31,87]. The ensuing sections focus on a fourth class of catalysts derived from metal amine metallates (MAM) [88].

MAM are heterometallic metal oxygen complexes of the formula (ML)(MoO$_4$), where M is a divalent promoter metal such as Co, L is one or more polydentate chelating ligands with a total denticity of six. The preparation of this class of complexes has been detailed elsewhere [88]. The stoichiometry is such that there can be multiple promoter and primary metals, e.g., $(M_zM^*_{1-z}L)(Mo_yW_{1-y}O_4)$ where M* is a second promoter metal and $0 \leq y \leq 1$. The presence of a second promoter metal can generate a synergistic effect, as has been demonstrated for the metal amine thiomolybdate system, $(M_zM^*_{1-z}L)(MoS_4)$, where M = Fe and M* = Co or Ni [31].

7.1. Pretreatment of metal amine metallates

In the following, ethylenediamine (en) is chosen as a bidentate ligand. We use Co(en)$_3$MoO$_4$ as an example to show some general characteristics of the MAM materials and how they are converted into bulk sulfide catalysts. Prior to sulfiding, Co(en)$_3$MoO$_4$ is thermally decomposed under flowing nitrogen. Fig. 10 shows that for high BET surface areas, the preferred temperature range is 370–400 °C. Thermogravimetric analyses indicated that the weight loss occurs at two different temperatures (250 and 370 °C), indicative of a stepwise loss of the amine ligand. X-ray
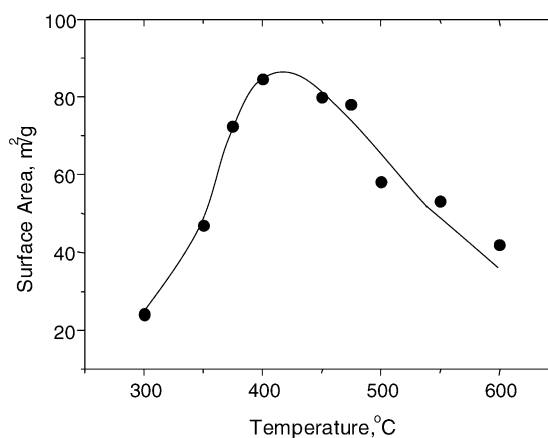

Fig. 10. BET surface area vs. decomposition temperature under nitrogen for Co(en)$_3$MoO$_4$.

diffraction (XRD) pattern of decomposed $Co(en)_3MoO_4$ showed that the resulting mixed metal oxide is essentially amorphous.

The resulting high surface area solid was typically sulfided with a 10–15% H_2S-in-H_2 mixture at 400 °C, even though MAM can be completely sulfided at temperatures much below than 400 °C. The heat release from gas sulfiding of MAM is far greater than that observed with commercial supported catalysts [89].

7.2. Diluted metal amine metallates

A constraint on MAM is that $r = M/(Mo + M) = 0.5$. To achieve $r < 0.5$, two approaches have been pursued based on a dilution hypothesis. One is to incorporate a "diluent" metal M' into the structure to form $(M_zM'_{1-z}L)(MoO_4)$ where M' by itself has little or no promotion effect. The other approach is discussed in Section 7.5.

A specific example of the diluted MAM materials is $Ni_{0.5}Mn_{0.5}(en)_3MoO_4$ in which manganese serves as the diluent metal. This material was converted into a bulk sulfide following the same pretreatment procedures described above. For comparison, a bulk sulfide was also prepared from $Ni(en)_3MoO_4$. The bulk $Ni_{0.5}Mn_{0.5}Mo$ and NiMo sulfides were tested against catalyst A with a feed containing 1.5 wt.% DBT (2600 ppmw S) in dodecane. The catalyst packing densities in the reactor were 1.2 g/cc for bulk catalysts and 0.8 g/cc for catalyst A. Table 1 shows the results obtained at 285 °C and 3.21 MPa. Catalyst A gave essentially 100% HDS, indicating that the catalyst may be underutilized. It was subsequently tested at 275 °C, which yielded a 96% HDS—still much higher than the 89.6% HDS obtained with $Ni_{0.5}Mn_{0.5}Mo$ at a higher temperature of 285 °C. Evidently, both bulk catalysts are much less active than catalyst A for DBT HDS.

A reverse trend was observed upon switching to a feed containing 1.7 wt.% 4-ethyldibenzothiophene (4EDBT, 2600 ppmw S) in dodecane. As Table 2 indicates, the bulk $Ni_{0.5}Mn_{0.5}Mo$ catalyst, with its high hydrogenation power ($\gamma = 11$), is far more active than catalyst A. Both bulk $Ni_{0.5}Mn_{0.5}Mo$ and NiMo sulfides can desulfurize 4EDBT more readily than they desulfurize DBT. The contrast is especially striking for $Ni_{0.5}Mn_{0.5}Mo$. Note also that the bulk $Ni_{0.5}Mn_{0.5}Mo$ sulfide is a superior catalyst than NiMo for the HDS of both DBT and 4EDBT. Although not shown here, the bulk MnMo catalyst derived from $Mn(en)_3MoO_4$ is much less active than the bulk NiMo catalyst.

The important point here is that 4EDBT can be more easily desulfurized than DBT over highly hydrogenative

Table 1
HDS of DBT at 285 °C, 3.21 MPa, and 5 WHSV

Catalyst	% HDS	γ
A	≥100	∼0.4
NiMo	72	2.0
$Ni_{0.5}Mn_{0.5}Mo$	89.6	2.9

Table 2
HDS of 4EDBT at 285 °C, 3.21 MPa, 5 WHSV

Catalyst	% HDS	γ
A	81.5	0.8
NiMo	80.5	6.9
$Ni_{0.5}Mn_{0.5}Mo$	97.3	11

transition metal sulfides (i.e., here DBT is more refractory than 4EDBT!). Presumably, $Ni_{0.5}Mn_{0.5}Mo$ has a high surface density of β sites. Landau et al. [90] reported that 46DMDBT desulfurizes faster than DBT on a sulfided NiW/SiO_2 catalyst; the reverse is true on a CoMo/Al_2O_3 catalyst. The toluene hydrogenation activity of NiW/SiO_2 is ten times that of CoMo/Al_2O_3.

We further tested $Ni_{0.5}Mn_{0.5}Mo$ for the HDS of a more-hindered molecule, 46DEDBT (1.7 wt.% 46DEDBT in dodecane), against catalyst B (NiMo/Al_2O_3) at 265 °C and 1.83 MPa. Fig. 11 depicts $\ln(S_p/S_f)$ versus 1/WHSV, which shows that catalyst B exhibits pseudo-first-order behavior, suggesting a low site coverage (similar to catalyst A). In contrast, $Ni_{0.5}Mn_{0.5}Mo$ shows a concave downward behavior, indicative of a strong adsorption. If the data are fitted with $(WHSV)dS/d\tau = -kS/(1 + KS)$, then $k = 52.4$ and $K = 42.6$ ($S_f = 0.227$ wt.%). With $KS_f \gg 1$, the overall HDS kinetics can be approximated by a small fractional order, implying a dense coverage of the active sites. Fig. 11 also shows the data for a bulk Co-promoted MoS_2 catalyst to be discussed in Section 7.5.

That the bulk $Ni_{0.5}Mn_{0.5}Mo$ sulfide and catalyst B give very different kinetics is a nontrivial point. It has practical implications with regard to quantification of catalyst activity (or sizing of reactor volume) and process configuration. In the former case, the catalyst activity ratio depends on the HDS level. This is shown in Fig. 12 where the activity ratio R (activity of $Ni_{0.5}Mn_{0.5}Mo$/activity of catalyst B) is a strong increasing function of percent HDS. That is, the advantage of the $Ni_{0.5}Mn_{0.5}Mo$ catalyst becomes more pronounced as the HDS level gets deeper. If we were dealing with the case

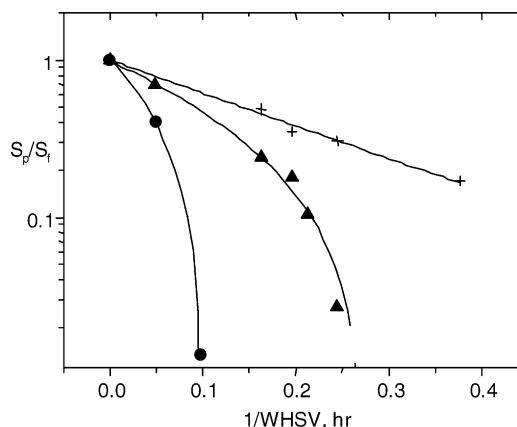Fig. 11. $\ln(S_p/S_f)$ vs. 1/WHSV for bulk $Ni_{0.5}Mn_{0.5}Mo$ sulfide (▲), catalyst B (+), and bulk $Co_{0.75}Mo$ sulfide (●); 1.7 wt.% 46DEDBT in dodecane; 1.83 MPa, 265 °C, 116 cc H_2/cc liquid.
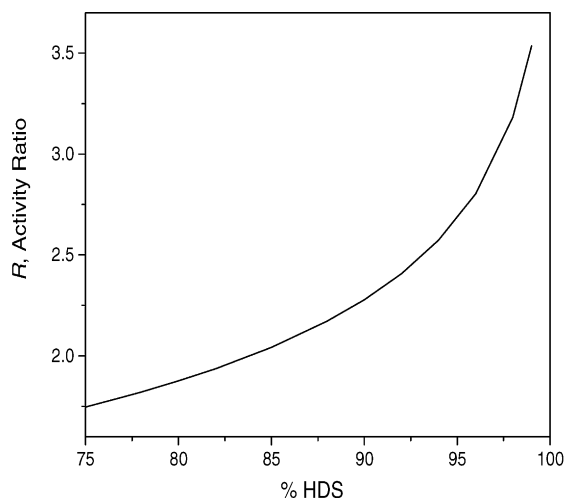
Fig. 12. Activity ratio R of $Ni_{0.5}Mn_{0.5}Mo$ to catalyst B for the HDS of 46DEDBT; 1.83 MPa, 265 °C, 116 cc H_2/cc liquid.

where two catalysts have the same reaction order (e.g., catalysts A and B), then the activity ratio (or rate constant ratio) is independent of the HDS level.

As for process configuration, the above results (Tables 1 and 2, Fig. 11) indicate that a synergy should result if the $Ni_{0.5}Mn_{0.5}Mo$ sulfide and a commercial catalyst are used together in a stacked bed. The preferred stacking order is to place the commercial catalyst upstream. This is indeed realized in real feed experiments [91,92], as summarized below.

7.3. Stacked bed studies

The comparative tests were carried out with an LCO (16.5° API, 1.35 wt.% S, and 715 ppmw N) at 2.38 MPa, 329 °C, and 1.0 LHSV. A commercial CoMo catalyst (catalyst C) was used. For comparison, the following base-case runs were conducted in: (1) a stacked bed in which $Ni_{0.5}Mn_{0.5}Mo$ was upstream of catalyst C, (2) a mixed bed in which the two catalysts were uniformly mixed, and (3) two single beds, one containing $Ni_{0.5}Mn_{0.5}Mo$, the other catalysts C. In the stacked- and mixed-bed experiments, each constituent catalyst occupied 50% of the bed volume. Table 3 summarizes the volumetric activities in terms of the second-order HDS rate constant (k_{HDS}) and the first-order HDN rate constant (k_{HDN}). The designation catalyst-C/ $Ni_{0.5}Mn_{0.5}Mo$ means that catalyst C is placed upstream of $Ni_{0.5}Mn_{0.5}Mo$.

The following observations can be made. (1) The catalyst-C/$Ni_{0.5}Mn_{0.5}Mo$ stacking order displays the highest synergy. (2) Either mixed- or stacked-bed (regardless of stacking order) performs better (HDS and HDN) than would be expected from the weighted sum of the activities of the constituent catalysts. (3) $Ni_{0.5}Mn_{0.5}Mo$ by itself, due to its low activity for desulfuring non-β-DBTs (Table 1), has a lower overall HDS activity than catalyst C. But it is a very active HDN catalyst because of its strong hydrogenation functionality. (4) For HDS, the catalyst-C/$Ni_{0.5}Mn_{0.5}Mo$ stacked bed is the only dual-catalyst bed that outperforms the single bed containing catalyst C. (5) In terms of HDS performance, the mixed bed falls in between the two stacked beds.

The preceding paragraphs show the advantage of a certain stacking order that plays the strength of each constituent catalyst in a synergistic fashion. The genesis of the synergy, simply put, is that it pays to do some prehydrotreating (HDS of non-β-DBTs, HDN, hydrogenation of PNA) over a conventional catalyst. Even a modest HDN level in the upstream zone goes a long way toward boosting $Ni_{0.5}Mn_{0.5}Mo$'s activity for desulfurizing β-DBTs. Also, the highly hydrogenative $Ni_{0.5}Mn_{0.5}Mo$ may be relatively insensitive to the H_2S generated from the HDS of non-β-DBTs over the upstream catalyst. The possibility that $Ni_{0.5}Mn_{0.5}Mo$ may actually benefit from H_2S cannot be ruled out with certainty.

The synergy observed with the $Ni_{0.5}Mn_{0.5}Mo$/catalyst-C configuration may be explained by the high HDN and hydrogenation activities of $Ni_{0.5}Mn_{0.5}Mo$, which mitigate the poisoning effects of nitrogen and aromatics on catalyst C.

7.4. Catalyst characterization

Here, the term predecessor refers to the material obtained after the thermal decomposition of MAM (precursor) but prior to sulfiding. The materials after sulfiding are called bulk catalysts. Thus, the predecessor of the active $Ni_{0.5}Mn_{0.5}Mo$ bulk catalyst is prepared from the thermal decomposition of $Ni_{0.5}Mn_{0.5}(en)_3MoO_4$ under nitrogen.

X-ray photoemission spectroscopy (XPS) was used to characterize various solid materials. Table 4 shows the surface metal atomic ratios for $Ni_{0.5}Mn_{0.5}(en)_3MoO_4$, predecessor materials (decomposed at 350 and 400 °C), and the bulk catalyst after sulfiding at 350 °C. As can be seen, the Ni/Mo and Mn/Mo XPS atomic ratios for $Ni_{0.5}Mn_{0.5}(en)_3MoO_4$ are close to the expected bulk metals stoichiometry. The Ni/Mo

Table 3
Comparison of stacked, mixed, and single beds

Catalyst Bed	k_{HDS}	k_{HDN}
Catalyst-C/$Ni_{0.5}Mn_{0.5}Mo$	10.5	0.71
$Ni_{0.5}Mn_{0.5}Mo$/catalyst-C	6.6	0.55
Mixed bed	7.7	0.5
Catalyst C	7.8	0.33
$Ni_{0.5}Mn_{0.5}Mo$	4.3	0.48
Weighted sum of catalyst C and $Ni_{0.5}Mn_{0.5}Mo$	6.1	0.41

Table 4
XPS atomic ratios for $Ni_{0.5}Mn_{0.5}(en)_3MoO_4$, predecessor and bulk catalyst

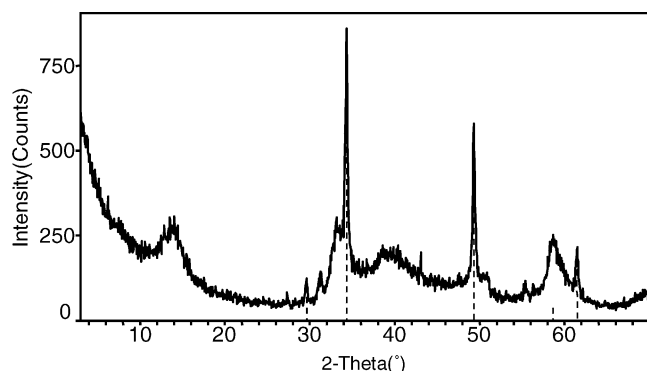| Treatment temperature (°C)	Ni/Mo	Mn/Mo
None	0.55	0.47
N_2—350	0.33	0.70
N_2—400	0.23	0.70
H_2S/H_2—350	3.7	1.10

Fig. 13. X-ray powder diffraction pattern of $Ni_{0.5}Mn_{0.5}Mo$ bulk sulfide. The vertical dashed lines indicate MnS.

Fig. 15. Histogram of micrograph for $Ni_{0.5}Mn_{0.5}Mo$; average number of stacking = 3.6.

ratio decreases and the Mn/Mo ratio increases slightly during the formation of the predecessor material, suggesting some surface reconstruction. The decreasing (Ni/Mo) ratio can probably be explained by aggregation of the metallic nickel crystallites.

Significant changes in the metal atomic ratios occurred when the predecessor materials were subsequently sulfided by the 350 °C H_2S-H_2 treatment. The promoter metal sulfide surface concentrations increase sharply, and the surface concentration of MoS_2-like species is reduced. Evidently, sulfiding causes a major restructuring of the catalyst surface. If the catalyst is composed of pseudo-bimetallic sulfide crystallites, then the XPS results indicates that the core of the crystallites is rich in MoS_2 and the surface region is enriched in nickel sulfide.

Fig. 13 shows the X-ray powder diffraction (XRD) pattern of the $Ni_{0.5}Mn_{0.5}Mo$ bulk sulfide (400 °C sulfiding temperature with 10% H_2S-in-H_2 mixture). One sees a
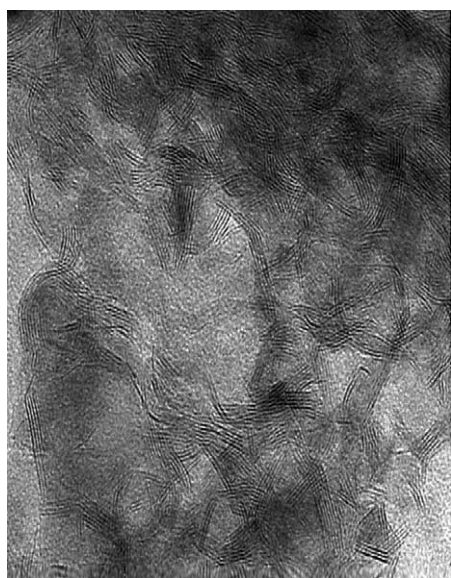
poorly crystalline MoS_2. The (0 0 2) peak at $2\theta = 14.4°$, which measures the stacking height of MoS_2, is noticeable. The dashed lines indicate crystalline MnS. Fig. 14 shows the high-resolution transmission electron micrograph of freshly sulfided $Ni_{0.5}Mn_{0.5}Mo$. The histogram shown in Fig. 15 indicates that the number of layers is mostly three and four, with an average number of stacking of 3.6.

7.5. Non-stoichiometric metal amine metallates

A second way of achieving $r < 1$ is to prepare the following catalyst precursor compound that formally is of the form "$[(ML)_xQ_{1-x}](MoO_4)$", with $0 < x < 1$. Here, Q is the conjugate acid of the ligand L, with a charge sufficient to balance the dinegative charge of the metallate anion. For example, if L is en, then Q can be $[(H)_2(en)_3]^{+2}$, $[(H)_2(en)]^{+2}$, $[(H)_2(en)_2]^{+2}$ and mixture thereof. For convenience, catalysts derived from this class of precursors are called non-stoichiometric bulk sulfides. As in the stoichiometric case, a second promoter or diluent metal can be added, that is, $[(ML)_x(M*L)_zQ_{1-x-z}](Mo_yW_{1-y}O_4)$, wherein $0 \leq z < 1$.

Briefly, the salt $(ML)_xQ_{1-x}(MoO_4)$ can be prepared by dissolving the appropriate amounts of ammonium molybdate and an M-containing salt such as nitrate in an aqueous solution containing excess ligand L. The desired salt is precipitated by addition of a suitable antisolvent such as methanol or ethanol with agitation and is recovered by filtration. The XRD patterns shown in Fig. 16 indicate that $Co(en)_3(MoO_4)$, $[Co(en)_3]_{0.75}Q_{0.25}(MoO_4)$, and $[Co_{0.75}Ni_{0.25}(en)_3](MoO_4)$ are isostructural. This suggests that the preparation most likely does not give rise to a physical mixture of $(ML)(MoO_4)$ and a metallate salt $Q(MoO_4)$. In the discussion that follows, we focus on $\{[Co(en)_3]_{0.75}Q_{0.25}\}(MoO_4)$ versus $[Co(en)_3](MoO_4)$ as catalyst precursors.

Prior to use, the precursor compounds were thermally decomposed under flowing nitrogen at 370 °C for 2 h and then sulfided at 400 °C for 2 h with a 10% H_2S-in-H_2 gas mixture. The mixed metal oxides resulting from the thermal decomposition are X-ray amorphous. The bulk sulfide
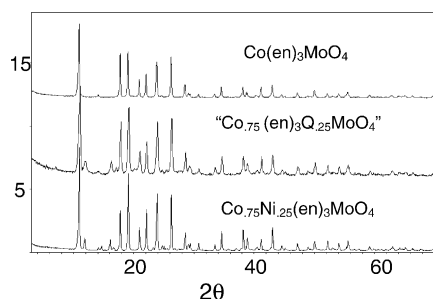

Fig. 14. High resolution transmission electron micrograph of bulk $Ni_{0.5}Mn_{0.5}Mo$ sulfide.

Fig. 16. X-ray powder diffraction patterns of "$[Co(en)_3]_{0.75}Q_{0.25}(MoO_4)$", $Co(en)_3(MoO_4)$, and $[Co_{0.75}Ni_{0.25}(en)_3](MoO_4)$.

Fig. 18. Histogram of micrograph for $Co_{0.75}Mo$; average number of stacking = 2.6.

catalysts prepared from $[Co(en)_3]_{0.75}Q_{0.25}(MoO_4)$ and $Co(en)_3(MoO_4)$ are denoted as $Co_{0.75}Mo$ and CoMo, respectively. Fig. 17 shows the XRD pattern of $Co_{0.75}Mo$, indicating a poorly crystalline MoS_2 and crystalline Co_9S_8. The (0 0 2) peak is almost absent despite the high sulfiding temperature used. The histogram shown in Fig. 18 indicates that MoS_2 crystallites have an average number of stacking of 2.6.

The activity of $Co_{0.75}Mo$, as shown in Fig. 11, is higher than that of $Ni_{0.5}Mn_{0.5}Mo$ for desulfurizing 46DEDBT. The more concave downward behavior of $Co_{0.75}Mo$ suggests that more 46DEDBT is adsorbed on $Co_{0.75}Mo$ than on $Ni_{0.5}Mn_{0.5}Mo$. Indeed, when the data for $Co_{0.75}Mo$ are plotted as (S_p/S_f) versus 1/WHSV, a straight line results (not shown), indicating a zero-order reaction and hence a full site coverage.

Fig. 19 contrasts the response of $Co_{0.75}Mo$ to H_2 pressure against that of catalyst A at 265 °C and 5.1 WHSV with a feed containing 0.8 wt.% 46DEDBT. At 1.83 MPa (250 psig), the $Co_{0.75}Mo$ catalyst achieves complete sulfur removal with $\gamma = 19$. It yields a high 70% HDS at a pressure as low as 0.79 MPa (100 psig), versus 18% for catalyst A. The "parent" catalyst, bulk CoMo sulfide, gives a 62% HDS. Thus, $Co_{0.75}Mo$ and CoMo both have very high *intrinsic* activities for desulfurizing a sulfur heterocycle with steric hindrance as severe as 46DEDBT at low hydrogen pressures. By "intrinsic" is meant that the activity is
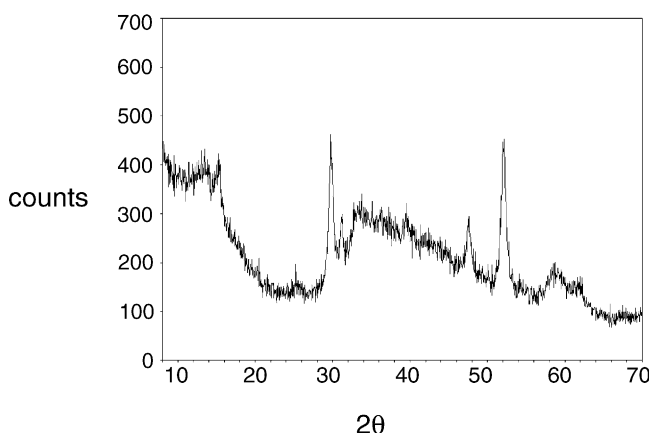
measured under conditions free of any competitive adsorption effect.

7.6. Geometric considerations

As noted earlier, Type I Co-Mo-S crystallites on commercial catalysts are single-layer MoS_2 crystals, whereas Type II crystallites have three to five stacked layers. There is evidence that the metal-sulfur bond strength for Type II sites is lower than that for Type I sites [7]. The size of DBT is comparable to that of a Type I crystallite. Commercial catalysts are quite selective toward DBT HDS compared to bulk sulfide catalysts. Whitehurst et al. [9] argued that the alignment of β-DBTs along Type I crystal's edge is quite limited. The sites on a Type II crystal are much more accessible and hence presumably more active for the HDS of β-DBTs. Both types, to a varying degree, are influenced by Mo-O-Al interactions. Carbon [9] and silica [90] have been used to mitigate the support effect.

The foregoing geometric consideration suggests that the relatively small MoS_2-like slabs in the bulk $Co_{0.75}Mo$ and $Ni_{0.5}Mn_{0.5}Mo$ sulfide catalysts are relatively accessible as

Fig. 17. X-ray powder diffraction pattern of $Co_{0.75}Mo$ bulk sulfide.
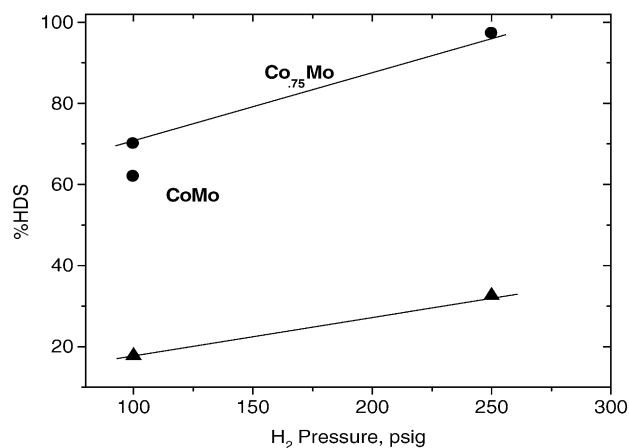

Fig. 19. 46DEDBT HDS activities of bulk $Co_{0.75}Mo$ sulfide and catalyst A as functions of hydrogen pressure; 265 °C and 5.1 WHSV, 0.8 wt.% 46DEDBT in dodecane.

far as β-DBTs adsorption is concerned. Moreover, they are free of the undesirable Mo–O–Al linkages. Thus, the bulk sulfide catalysts appear to have a high surface density of β sites that are rare on commercial Co(Ni)Mo/Al$_2$O$_3$ catalysts. Given the molecular complexity of petroleum distillates, for maximum activity and/or selectivity, there may be an optimum distribution of MoS$_2$ slab sizes. Obviously, the geometric effect (e.g., MoS$_2$ stacking height) is only part of the puzzle. Many questions remained to be answered, such as the local compositions and structure and their effects on catalytic properties.

8. Concluding remarks

There is considerable variation in reactivity among β-DBTs [21]. Removing the last, say, 200–300 ppmw sulfur from difficult-to-treat raw or prehydrotreated distillates means desulfurization of the most hindered β-DBTs. This requires metal sulfide (e.g., MoS$_2$-based) catalysts with strong hydrogenation functionality. However, highly hydrogenative metal sulfide catalysts in general are particularly prone to poisoning by nitrogen species (e.g., alkylcarbazoles), which are the most potent poison in the ultra-low sulfur regime. Such catalysts are potentially limited by the supply of surface hydrogen. These limiting factors become more important in low-pressure operation.

Furthermore, catalysts of high hydrogenation functionality are not ideally suited for the HDS of non-β-DBTs, which can be more efficiently desulfurized over catalysts with strong hydrogenolysis functionality (e.g., commercial catalysts). An obvious question then is whether these two catalyst types can be used together in a synergistic manner. In this study, we have found that bulk metal sulfides derived from metal amine metallates are highly hydrogenative and as such show very high intrinsic activities and selectivities for the HDS of β-DBTs. They are best used in a stacked bed in which a commercial catalyst is placed in the upstream zone to prehydrotreat the feed.

Acknowledgement

References

[1] C. Song, Catal. Today 86 (2003) 211.
[2] M. Houalla, N.K. Nag, A.V. Sapre, D.H. Broderick, B.C. Gates, AIChE J. 24 (1978) 1015.
[3] M. Houalla, D.H. Broderick, A.V. Sapre, N.K. Nag, V.H.J. de Beer, B.C. Gates, H. Kwart, J. Catal. 61 (1980) 523.
[4] R. Prins, V.H.J. DeBeer, G.A. Somorjai, Catal. Rev. Sci. Eng. 31 (1989) 1.
[5] M.J. Girgis, B.C. Gates, Ind. Eng. Chem. Res. 30 (1991).
[6] Startsev, Catal. Rev. Sci. Eng. 37 (1995) 353.
[7] H. Topsøe, B.S. Clausen, F.E. Massoth, Hydrotreating Catalysis, Springer-Verlag, 1996.
[8] S. Eijsbouts, Appl. Catal. A: Gen. 158 (1997) 53.
[9] D.D. Whitehursts, T. Isoda, I. Mochida, Adv. Catal. 42 (1998) 345.
[10] T. Kabe, A. Ishihara, W. Qian, Hydrodesulfurization and Hydrodenitrogenation, Wiley-VCH, New York, 1999.
[11] M. Sun, D. Nicosia, R. Prins, Catal. Today 86 (2003) 173.
[12] K. Choi, N. Kunisada, Y. Korai, I. Mochida, K. Nakano, Catal. Today 86 (2003) 277.
[13] C. Song, X. Ma, Appl. Catal. B: Environ. 41 (2003) 207.
[14] M. Breysse, G. Djega-Mariadassou, S. Pessayre, C. Geantet, M. Vrinat, G. Pérot, M. Lemaaire, Catal. Today 84 (2003) 129.
[15] T.C. Ho, J. Catal. 219 (2003) 442.
[16] K. Sakanishi, T. Nagamatsu, I. Mochida, D.D. Whitehurst, J. Mol. Catal. A: Chem. 155 (2000) 101.
[17] H. Farag, K. Sakanishi, I. Mochida, D.D. Whitehurst, Energy Fuel 13 (1999) 449.
[18] H. Farag, I. Mochida, K. Sakanishi, Appl. Catal. A: Gen. 194 (2000) 147.
[19] F. Bataille, J.L. Lemberton, P. Michand, G. Perot, M. Vrinat, M. Lemaire, E. Schulz, M. Breysse, S. Kasztelan, J. Catal. 191 (2000) 409.
[20] H. Topsøe, B.S. Clausen, N.Y. Topsøe, P. Zeuthen, et al. in: D.L. Trimm (Ed.), Catalysts in Petroleum Refining, Elsevier, 1990.
[21] M. Macaud, A. Milenkovic, E. Schulz, M. Lemaire, M. Vrinat, J. Catal. 193 (2000) 255.
[22] Y. Saih, K. Segawa, Catal. Today 86 (2003) 61.
[23] X. Ma, K. Sakanishi, T. Isoda, I. Mochida, Pap. Am. Chem. Soc. Prepr. Div. Petrol. Chem. 39 (1994) 622.
[24] T. Kabe, A. Ishihara, Q. Zhang, Appl. Catal. A: Gen. 97 (1993) 1.
[25] V. Meille, E. Schulz, M. Lemaire, M. Vrinat, J. Catal. 170 (1997) 29.
[26] J. Mijoin, G. Pérot, F. Bataille, J.L. Lemberton, M. Breysse, S. Kasztelan, Catal. Lett. 71 (2001) 139.
[27] H. Pines, The Chemistry of Catalytic Hydrocarbon Conversions, Academic Press, New York, 1981, pp. 99–100.
[28] N. Hermann, M. Brorson, H. Topsøe, Cata. Lett. 65 (2000) 169.
[29] T.C. Ho, A.J. Jacobson, R.R. Chianelli, R.F. Lund, J. Catal. 138 (1992) 351.
[30] T.C. Ho, Ind. Eng. Chem. Res. 32 (1993) 1568.
[31] T.C. Ho, A.J. Jacobson, R.R. Chianelli, Appl. Catal. A: Gen. 114 (1994) 127.
[32] E. Olguin, M. Vrinat, Appl. Catal. A: Gen. 170 (1998) 195.
[33] C. Thomas, L. Vivier, A. Travert, F. Maugé, S. Kasztelan, G. Pérot, J. Catal. 179 (1998) 495.
[34] E. Lecrenay, I. Mochida, Stud. Surf. Sci. Catal. 106 (1997) 333.
[35] T.C. Ho, Appl. Catal. A: Gen. 244 (2003) 115.
[36] T.C. Ho, G.E. Markley, Appl. Catal. 267 (2004) 245.
[37] S. Wold, P. Geladi, K. Esbensen, J. Ohman, J. Chemom. 1 (1987) 41.
[38] H. Schultz, W. Bohringer, P. Wallen, P.E. Oasmanor, Catal. Today 49 (1999) 87.
[39] S.S. Shih, S. Mizrahi, L.A. Green, M.S. Sarli, Ind. Chem. Res. 31 (1992) 1232.
[40] U.T. Turaga, G. Wang, X. Ma, C. Song, Prepr. ACS Div. Fuel Chem. 48 (2003) 550.
[41] T.C. Ho, Catal. Rev. Sci. Eng. 30 (1988) 117.
[42] S.D. Sumbogo Murti, H. Yang, K.H. Choi, Y. Korai, I. Mochida, Appl. Catal. A: Gen. 252 (2003) 331.
[43] P. Zeuthen, K.G. Knudsen, P.D. Whitehurst, Catal. Today 65 (2001) 307.
[44] P. Wiwel, K. Kundsen, P. Zeuthen, D. Whitehurst, IEC Res. 39 (2000) 533.
[45] F. van Looij, P. van der Laan, W.H.J. Stork, D.J. Di Camillo, J. Swain, Appl. Catal. A: Gen. 170 (1980) 1.

[46] I. Igniatiadis, M. Kuroki, P. Arpino, J. Chromatogr. 366 (1986) 251.
[47] J.M. Schmitter, I. Igniatiadis, M. Dorbon, P. Arpino, G. Guiochon, H. Toulhout, A. Huc, Fuel 63 (1984) 557.
[48] M. Dorbon, I. Igniatiadis, J.M. Schmitter, P. Arpino, G. Guiochon, H. Toulhout, A. Huc, Fuel 63 (1984) 565.
[49] G.C. Laredo, S. Leyva, R. Alvarez, M.T. Mares, J. Castillo, J.L. Cano, Fuel 81 (2002) 1341.
[50] S. Shin, K. Sakanishi, I. Mochida, Energy Fuels 14 (2000) 539.
[51] S.K. Bej, A.K. Dalai, J. Adjaye, Energy Fuels 15 (2001) 377.
[52] S.C. Kim, F.E. Massoth, J. Catal. 189 (2000) 70.
[53] H. Farag, K. Sakanishi, M. Kouzu, A. Matsumura, Y. Sugimoto, I. Saito, Ind. Eng. Chem. Res. 42 (2003) 306.
[54] J. Leglise, J.N.M. van Gestel, L. Finot, J.C. Duchet, J.L. Dubois, Catal. Today 45 (1998) 347.
[55] T. Kabe, K. Akamatsu, A. Ishihara, S. Otsuki, M. Godo, Q. Zhang, W. Qian, Ind. Eng. Chem. 36 (1997) 5146.
[56] J. Yao, H.M. Sebastian, H.M. Lin, K.C. Chao, Fluid Phase Equilib. 1 (1977/1978) 293.
[57] U. Plocker, H. Knapp, J. Prausnitz, Ind. Eng. Chem. Proc. Des. Dev. 17 (1978) 224.
[58] J.J. Simnick, C.C. Lawson, H.M. Lin, K.C. Chao, AIChE J. 23 (1977) 469.
[59] H.M. Sebastian, H.M. Lin, K.C. Chao, AIChE J. 27 (1981) 138.
[60] H.M. Sebastian, J. Yao, H.M. Lin, K.C. Chao, J. Chem. Eng. Data 23 (1978) 167.
[61] M. Muroi, S. Nakagawa, R. Shiba, M. Miura, M. Nomura, Sekiyu Gakkaishi 41 (1998) 232.
[62] P.A. Rautanen, J.R. Alttamaa, A.O.I. Krause, Ind. Eng. Chem. Res. 39 (2000) 4032.
[63] T.C. Ho, Catal. Lett. 89 (2003) 21.
[64] M.D. Ackerson, M.S. Byars, US Patents 6,123,835 (2000) and 6,428,686 (2002).
[65] H. Farag, D.D. Whitehurst, K. Sakanishi, I. Mochida, Catal. Today (1999) 50.
[66] P. Steiner, E.A. Blekkan, Fuel Process. Technol. 79 (2002) 1.
[67] F.E. Massoth, S.C. Kim, Catal. Lett. 57 (1999) 129.
[68] S.H. Yang, C.N. Satterfield, Ind. Eng. Chem. Proc. Des. Dev. 23 (1984) 20.
[69] T.C. Ho, A.R. Katritzky, S.J. Cato, Ind. Eng. Chem. Res. 31 (1992) 1589.
[70] T. Koltai, M. Macaud, A. Guevara, E. Schulz, M. Lemaire, R. Bacaud, M. Vrinat, Appl. Catal. A: Gen. 231 (2002) 253.
[71] T.C. Ho, D. Nguyen, J. Catal. 222 (2004) 450.
[72] R. Ramachandran, F.E. Massoth, Can. J. Chem. Eng. 60 (1982) 17.
[73] F.E. Massoth, J. Miciukiewicz, J. Catal. 101 (1982) 505.
[74] Q. Zhang, A. Ishihara, T. Kabe, Sekiyu Gakkaishi 39 (1996) 410.
[75] T. Kabe, Y. Aoyama, D. Wang, A. Ishihara, W. Qian, M. Hosoya, Q. Zhang, Appl. Catal. A: Gen. 209 (2001) 237.
[76] T. Kabe, A. Ishihara, H. Tajima, Ind. Eng. Chem. Res. 31 (1992) 1577.
[77] D. Whitehurst, M. Brorson, K. G. Knudsen, P. Zeuthen, B. H. Cooper, EP Patent 1,057,897, A2, 2000.
[78] A. Milenkovic, E. Schulz, V. Meille, D. Lofreda, M. Forissier, M. Vrinat, P. Sautet, M. Lemaire, Energy Fuels 13 (1999) 881.
[79] X. Ma, L. Sun, C. Song, Catal. Today 77 (2002) 107.
[80] R.T. Yang, A.J. Hernandez-Maldonado, F.H. Yang, Science 302 (2003) 79.
[81] E.I. Stiefel, T.R. Halbert, C.L. Coyle, W.H. Pan, T.C. Ho, R.R. Chianelli, M. Daage, Polyhedron 8 (1989) 1625.
[82] T.C. Ho, W.H. Pan, US Patent 4,514,517, 1985.
[83] E.I. Stiefel, W.H. Pan, R.R. Chianelli, T.C. Ho, US Patent 4,581,125, 1986.
[84] M. Angulo, F. Mauge, J.C. Duchet, J.C. Lavalley, Bull. Soc. Chim. Belg. 96 (1987) 925.
[85] T.R. Halbert, E.I. Stiefel, R.R. Chianelli, T.C. Ho, US Patent 4,839,326.
[86] T.R. Halbert, T.C. Ho, E.I. Stiefel, R.R. Chianelli, M. Daage, J. Catal. 130 (1991) 116.
[87] T.C. Ho, A.R. Young, A.J. Jacobson, R.R. Chianelli, US Patent 4,591,429, 1986.
[88] T.C. Ho, L.E. McCandlish, US Patent 4,595,672, 1986.
[89] T.C. Ho, S.C. Reyes, Chem. Eng. Sci. 45 (1990) 2633.
[90] M.V. Landau, L. Vradman, M. Herkowitz, D. Yitzhaki, in: B. Delmon, G.F. Froment, P. Grange (Eds.), Hydrotreatment and Hydrocracking of Oil Fractions, Elsevier, 1999.
[91] T.C. Ho, US Patent, 4,902,404, 1990.
[92] T.C. Ho, US Patent 4,973,397, 1990.